AD-A133 089   THE EFFECT OF FIELD INDEX FLUCTUATIONS ON THE DYNAMICS   1/1
              OF A HIGH CURRENT... (U) NAVAL RESEARCH LAB WASHINGTON DC
              C AGRITELLIS ET AL. 14 SEP 83 NRL-MR-5141

UNCLASSIFIED   F/G 9/2   NL
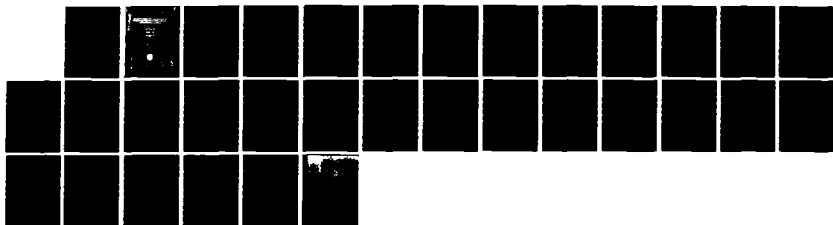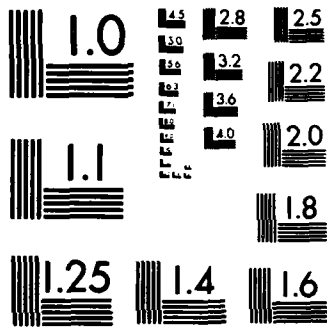
MICROCOPY RESOLUTION TEST CHART

NATIONAL BUREAU OF STANDARDS-1963-A
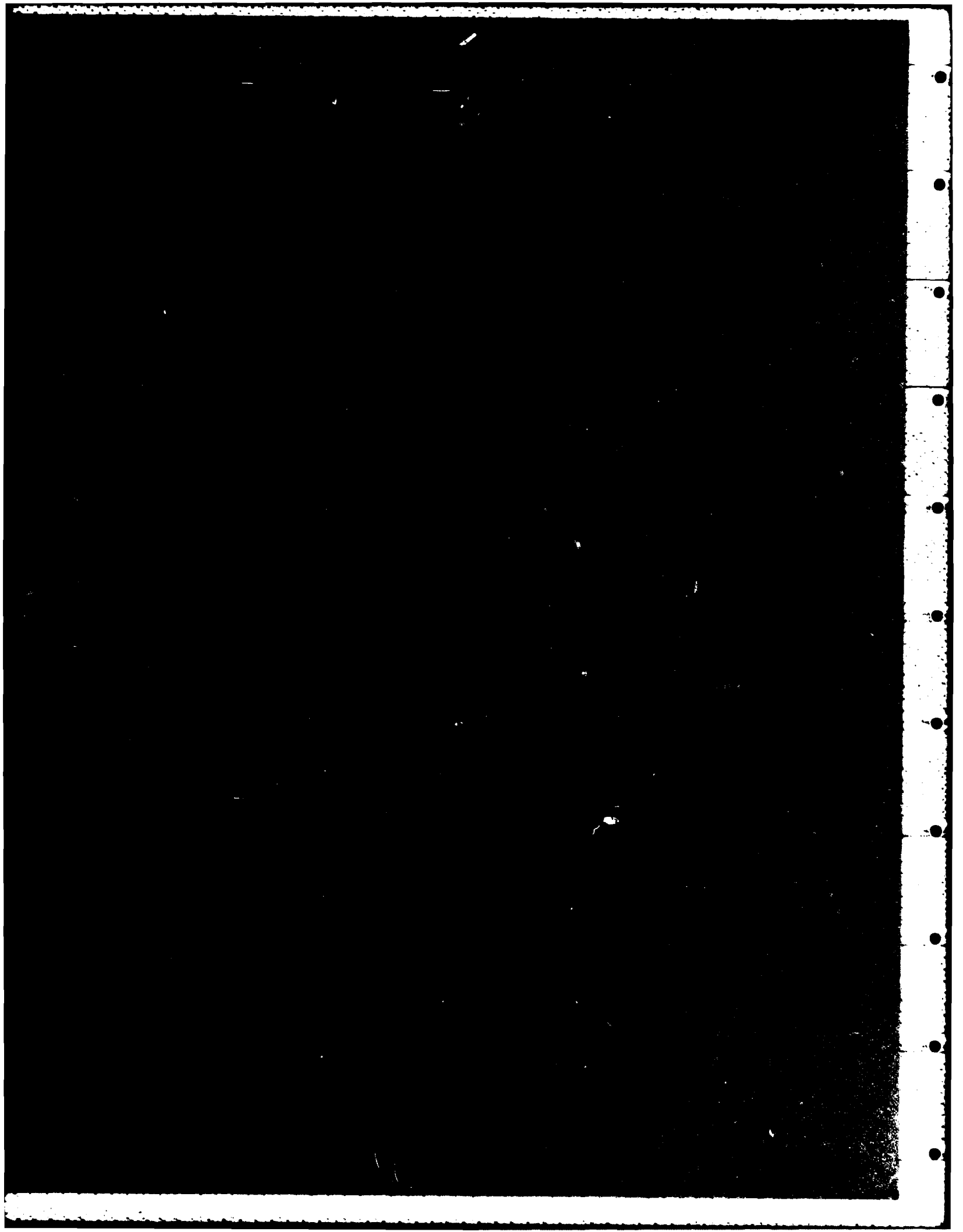
REPORT DOCUMENTATION PAGE	READ INSTRUCTIONS BEFORE COMPLETING FORM

1. REPORT NUMBER	2. GOVT ACCESSION NO.	3. RECIPIENT'S CATALOG NUMBER
NRL Memorandum Report 5141	*A133089*	

4. TITLE (and Subtitle)	5. TYPE OF REPORT & PERIOD COVERED
THE EFFECT OF FIELD INDEX FLUCTUATIONS ON THE DYNAMICS OF A HIGH CURRENT ELECTRON RING IN A MODIFIED BETATRON ACCELERATOR	Interim report on a continuing NRL problem.
	6. PERFORMING ORG. REPORT NUMBER

7. AUTHOR(s)	8. CONTRACT OR GRANT NUMBER(s)
C. Agritellis,* S.J. Marsh,** and C.A. Kapetanakos	

9. PERFORMING ORGANIZATION NAME AND ADDRESS	10. PROGRAM ELEMENT, PROJECT, TASK AREA & WORK UNIT NUMBERS
Naval Research Laboratory Washington, DC 20375	61153N; RR011-09-41; 47-1484-0-3

11. CONTROLLING OFFICE NAME AND ADDRESS	12. REPORT DATE
Office of Naval Research Arlington, VA 22217	September 14, 1983
	13. NUMBER OF PAGES
	30

14. MONITORING AGENCY NAME & ADDRESS(if different from Controlling Office)	15. SECURITY CLASS. (of this report)
	UNCLASSIFIED
	15a. DECLASSIFICATION/DOWNGRADING SCHEDULE

16. DISTRIBUTION STATEMENT (of this Report)

Approved for public release; distribution unlimited.

17. DISTRIBUTION STATEMENT (of the abstract entered in Block 20, if different from Report)

18. SUPPLEMENTARY NOTES

*Present address: Science Applications, Inc., McLean, VA 22102
**Present address: Sachs/Freeman Associates, Bowie, MD 20715

19. KEY WORDS (Continue on reverse side if necessary and identify by block number)

Modified betatron
Betatron
Accelerators
High current accelerators

20. ABSTRACT (Continue on reverse side if necessary and identify by block number)

Analytical and computer simulation results are reported on the effect of the external field index fluctuations on the dynamics of a high current electron ring in a modified betatron. These non-linear studies clearly demonstrate that the external field index fluctuations are, in general, harmless to the high current ring. In addition, it was found that a small (1%) temperature spread parallel to the direction of propagation excites oscillations in the rms emittance, but the amplitude of these oscillations is substantially lower than in a conventional betatron.

DD FORM 1473 EDITION OF 1 NOV 65 IS OBSOLETE
1 JAN 73
S/N 0102-014-6601

CONTENTS

Accession For		
NTIS GRA&I	X	
DTIC TAB	☐	
Unannounced	☐	
Justification		
By		
Distribution/		
Availability Codes		
	Avail and/or	
Dist	Special	
A		

iii

THE EFFECT OF FIELD INDEX FLUCTUATIONS ON THE
DYNAMICS OF A HIGH CURRENT ELECTRON RING IN A
MODIFIED BETATRON ACCELERATOR

I. Introduction

The linear dynamics of a high current electron ring in a modified betatron geometry has been studied extensively[1-11] during the last few years. These studies are mainly motivated by extensive evidence suggesting that the modified betatron has the potential to confine high current electron rings, even in the presence of a substantial transverse emittance[12].

The modified betatron belongs to the class of cyclic induction accelerators, i.e., the electrons are accelerating by an inductive electric field. So far these different cyclic induction accelerators have been proposed: the conventional betatron[13-15], the modified betatron[1-11] and the stellatron[15]. The modified betatron includes in addition to the time varying betatron magnetic field that is responsible for the acceleration, a strong toroidal magnetic field that substantially improves the stability of the conventional betatron. In the stellatron, the addition of a stellarator field to the modified betatron substantially reduces the displacement of the orbit that is due to energy mismatch. However, beam trapping and resonances appear to be major and presently unsolved problems.

The non-linear dynamics of very tenuous electron rings in a modified betatron accelerator has been studied recently by Chernin[17]. His studies were limited to quadratic non-linearities in the absence of self-fields and image fields from the surrounding walls. For azimuthally symmetric fields, he concluded that the quadratic non-linearities are quite harmless to the electron ring. In this paper, we present computer simulation results which clearly demostrate that Chernin's conclusion is valid under much more general

conditions, i.e., for high current rings in the present of surrounding walls and strong non-linearities as for example when the spatial derivatives of the external field index are large.

II. Computer Simulation Results

a. Description of the particle in cell computer code.

The computer code has been described previously[8]. Here we provide a very brief summary with emphasis on a recent modification related to the initial loading of the particles. Briefly, the particle simulation code is 2D in configuration and 3D in velocity space. It computes self-consistently all self field, except the self B_θ field. This assumption is valid provided ν/γ is small. In addition the radiative term (displacement current) is ignored, i.e., the code uses the Darwin model for Maxwell's equations.

The electrostatic potential is computed from Poission's equation

$$\nabla^2 \Phi = \rho/\varepsilon_o, \tag{1}$$

and the magnetic vector potential from

$$\nabla^2 A_\theta - \frac{A_\theta}{r^2} = -\mu_o J_\theta, \tag{2}$$

with the boundary condition $\Phi = A_\theta = 0$ at the conducting wall.

Equations (1) and (2) are solved by Fourier decomposition in the z-direction and then by Gaussian elimination of the resultant tridiagonal matrix of equations obtained from a 3-point differencing scheme for ∇_r^2. The inverse Fourier transform yields A_θ and Φ on the grid. The particle velocities in the toroidal direction are obtained using the conservation of cannonical momentum. Therefore, the equation for A_θ is not properly time centered since the velocities from the previous time step are used to calculate the currents from the cannonical momenta. This method was chosen primarily for its speed and simplicity but care must be taken in applying the code when the inductive acceleration of particles in the toroidal direction is significant.

In several runs the particles were loaded in the code at t = o using a cylindrical K-V distribution. In these runs the electrons quickly acquired an "energy spread". This "thermalization" is due to the fact a cylindrical K-V distribution is not appropriate for high current electron rings that have large aspect ratio r_o/r_b, where r_o is the major and r_b the minor radii of the ring. The reason is that a cylindrical K-V distribution requires that the potential be the same on both the left and right side of the beam. However, in a actual ring there is a potential difference between the inner and outer edge. Thus, a ring that has been incorrectly initialized tries to attain a more physical distribution, but in the absence of dissipation this can be achieved only temporarily. In the process a spread in γ is developed, which is equivalent to temperature. In all the results presented in this paper the code was loaded at t = o correctly, i.e., taking into account the asymmetry of the potential across the ring.

b. Results without temperature in the azimuthal direction.

Figure 1 shows the modified betatron geometry and the system of coordinates that will be used in our subsequent discussion. The center of the electron ring is located away from the center of the minor cross-section of the torus and at a distance $\Delta = (\Delta r^2 + \Delta z^2)^{1/2}$. Results from the computer simulation are shown in Fig. 2. The various parameters for this run are listed in Table I. At t = o the 5 KA electron ring is located on the horizontal symmetry plane and at a distance Δ = 8 cm, i.e., half-way between the minor axis and the wall of the toroidal chamber. It is apparent from the small variations of the rings envelopes [Figs. 2a and 2b] that the ring is reasonably well matched. As shown in Table I the external field index n is constant and equal to 0.42. For such a value of n the linear theory predicts that the minor axis of the ring has two modes of oscillation, a slow (bounce frequency) and a fast (cyclotron frequency corresponding to the toroidal field). The orbit of the ring axis associated with the slow or bounce mode is approximately a circle that is centered around the ring's equilibrium position. Although the run was terminated before the ring could complete a full bounce period, it is clear from Fig. 2c that the center of the ring describes an orbit that is similar to that predicted by the theory. Both modes of oscillation are quite apparent. The radius of the fast mode ρ_f can be computed approximately from the expression $\rho_f = (v_\theta \varepsilon_N / r_b \Omega_\theta)$, where v_θ is the azimuthal velocity, ε_N is the normalized emittance, r_b is the ring radius

4

and Ω_θ the cyclotron frequency of the local toroidal magnetic field. The time interval between two successive arrows in the figure is 20 nsec.

The ring kinetic energy also oscillates with the two characteristic modes as may be seen in Fig. 2d. The variations of γ can be computed approximately by integrating the energy rate equation

$$mc^2 \frac{d\gamma}{dt} = - |e| \vec{v} \cdot \vec{E} = |e| v_\theta \frac{dA_\theta}{dt}, \qquad (3)$$

using for the self magnetic vector potential the expression

$$A_\theta^s = \frac{2I_r}{c} \left(1/2 + \ln (a/r_b) + \ln (1 - \Delta^2/_a 2)\right). \qquad (4)$$

In Eq. (4), I_r is the ring current, a is the minor radius of the torus and Δ is the distance between the ring's minor axis and that of the torus. It should be noticed that Eq. (4) does not include toroidal effects and therefore is valid only for low ν/γ.

Since $I_r = - |e| N v_\theta/_{2\pi r}$, where N is the total number of electrons in the ring and the external part of the magnetic vector potential remains constant, we get from Eqs. (3) and (4)

$$\gamma (t) - \gamma (o) = 2\nu_o \{\frac{r_o}{r(o)} \left(1/2 + \ln (a/r_b (o))+ \right.$$

$$\ln (1 - \Delta^2(o)/a^2)] - \frac{r_o}{r(t)} [1/2 + \ln (a/r_b(t)) + \ln (1 - \Delta^2(t)/_a 2)]\}, \qquad (5)$$

where ν_o is the Budker parameter at r_o, i.e.,

$$\nu_o = \frac{N}{2\pi r_o} \frac{|e|^2}{mc^2} .$$ (6)

In the fast mode γ changes through the transverse oscillations of the ring's envelope. Since in this fast time scale r and Δ remain approximately constant, Eq. (5) becomes

$$\gamma(t) - \gamma(o) = 2\nu_o \frac{r_o}{r} \ell n \left[r_b(t)/r_b(o) \right] .$$

In the slow mode γ changes mainly through the variation of the ring current, which results from the changing r. Since the contribution from the variation of r_b and Δ are in general small, Eq. (5) gives

$$\gamma(t) - \gamma(o) = 2\nu_o \, r_o \, \{1/2 + \ell n \, (a/r_b(o)) +$$
$$\ell n \, (1 - \Delta^2(o)/_a 2)] \, (\frac{1}{r(o)} - \frac{1}{r(t)}) .$$ (7)

Equation (7) predicts that $\gamma(t)$ decreases with $r(t)$. In addition, for the results of Fig. 2d, Eq. (7) predicts a reduction in γ between $t = o$ and $t = 80$ nsec of 0.18, which is in excellent agreement with the computer simulation results.

As it was stated before, the run shown in Fig. 2 was made using a constant external field index. The purpose of this run was to serve as a "bench mark" for the rest of the runs that were made with a variable external field

6

index. The radial profile of the betatron field and the variation of the external field index are shown in Fig. 3. The assumed variation is in effect greater than that expected to be present in a well designed device.

The effect of the external field index variation on the dynamics of the ring is shown in Fig. 4. The parameters of this run are listed in Table II and with the exception of the external field index are identical to those of run listed in Table I. By comparing Figs. (2) and (4) it may be concluded that the variation of the field index does not have a profound effect on the dynamics of the ring. Although some details are different the gross features of the two runs are very similar. The most pronounced new feature of the results in Fig. 4 is the slow time scale variation of the ring envelope. As the ring moves from its initial position at $z = o$ to $z \neq o$, the field index is reduced and the ring becomes unmatched, resulting in envelope oscillations.

Snap-shots of the minor cross section of the ring and the magnetic field lines corresponding to the total magnetic field are shown in Fig. 5. As can be easily computed, the zero magnetic field point occurs at $\sim r_{b/2}$.

Similar results to those shown in Fig. 4 were also obtained for smaller initial ring displacements $\Delta (o)$. Figure 6 shows the results for $\Delta (o) = 5$ cm. The various parameter of this run are listed in Table III. In all the runs we carefully avoided crossing the beam resonance, i.e., the radial frequency

$$\tilde{\omega}_r^2 = (\frac{\Omega_{oz}}{\gamma_o})^2 \ [\xi^2 - n \ (t) \ \xi - n_s r_b^2 /_a 2],$$

7

$$\text{where } \xi = [1 + 2 \, (\nu/_\gamma) \, (0.5 + \ln a/r_b)]^{-1}$$

was kept different than zero. The implications of crossing the resonance are presently under investigation.

·c. The effect of temperature

In the system of coordinates shown in Fig. 1, the equations describing the motion of individual electrons in a constant radius beam with $\Delta = o$ having an azimuthal energy spread $\Delta\gamma/_{\gamma_o}$ are

$$\ddot{\delta r} + \omega_r^2 \, \delta r - (\Omega_{o\theta}/\gamma_o) \, \Delta \, \dot{z} = \frac{c^2}{r_o} \frac{\Delta\gamma}{\gamma_o}, \qquad (8)$$

$$\ddot{\delta z} + \omega_z^2 \, \delta z + (\Omega_{o\theta}/\gamma_o) \, \dot{\delta r} = o, \qquad (9)$$

where $\omega_r^2 = (\Omega_{oz}/\gamma_o)^2 \, (1-n-n_s)$, $\omega_z^2 = (\Omega_{oz}/\gamma_o)^2 \, (n-n_s)$ and $\Delta\gamma = \gamma - \langle\gamma\rangle$ is the azimuthal energy spread in the beam. Equations (8) and (9) do not include the toroidal corrections in the fields and therefore are valid only for low ν/γ_o beams.

In the Larmor frame, i.e., a frame that rotates with a constant frequency $\Omega_L = 1/2 \, (\Omega_{o\theta}/\gamma_o)$, Eqs. (8) and (9) take the form

$$\ddot{\widehat{\delta r}} + K^2 \, \widehat{\delta r} = \frac{c^2}{r_o v_\theta^2} \frac{\Delta\gamma}{\gamma_o} \cos \left(\frac{\Omega_L s}{v_\theta}\right), \qquad (10)$$

$$\ddot{\widehat{\delta z}} + K^2 \, \widehat{\delta z} = \frac{c^2}{r_o v_\theta^2} \frac{\Delta\gamma}{\gamma_o} \sin \left(\frac{\Omega_L s}{v_\theta}\right), \qquad (11)$$

8

where

$$\hat{\delta r} = \cos\left(\frac{\Omega_L s}{v_\theta}\right) \delta r - \sin\left(\frac{\Omega_L s}{v_\theta}\right) \delta z,$$

$$\hat{\delta z} = \sin\left(\frac{\Omega_L s}{v_\theta}\right) \delta r + \cos\left(\frac{\Omega_L s}{v_\theta}\right) \delta z,$$

$K^2 = (\omega^2 + \Omega_L^2) / v_\theta^2$, $\omega^2 = \omega_r^2 = \omega_z^2$, i.e., $n=1/2$, $\hat{\delta r}' = \frac{d\hat{\delta r}}{ds}$, $s = r_o\theta$ and θ is the toroidal angle.

Equations (10) and (11) describe forced oscillations and have a resonance at $\omega = o$.

The solution of Eqs. (10) and (11), when K is independent of s is

$$\hat{\delta r} = [\hat{\delta r}(o) - \delta r_o] \cos Ks + \frac{\hat{\delta r}'(o)}{K} \sin Ks + \delta r_o \cos\left(\frac{\Omega_L s}{v_\theta}\right), \qquad (12)$$

and

$$\hat{\delta z} = \hat{\delta z}(o) \cos Ks + \frac{1}{K} [\hat{\delta z}'(o) - \delta r_o \Omega_L/v_\theta] \sin Ks + \delta r_o \sin\left(\frac{\Omega_L s}{v_\theta}\right), \quad (13)$$

where

$$\delta r_o = \frac{c^2}{r_o \omega^2} \frac{\Delta\gamma}{\gamma_o}. \qquad (14)$$

The rms beam emittance is defined by

$$\hat{\epsilon} = 4 \{ \langle \hat{\delta r}^2(t) \rangle \langle \hat{\delta r}'^2(t) \rangle - \langle \hat{\delta r}(t) \, \hat{\delta r}'(t) \rangle \}^{1/2}. \qquad (14)$$

Substituting Eqs. (12) and (13) into Eq. (14) and taking averages over a K-V distribution, we obtain

$$\frac{\hat{\epsilon}^2}{16} = \langle \hat{\delta r}^2(o) \rangle \langle \hat{\delta r}'^2(o) \rangle$$

$$\cdot + \delta r_o^2 \{ \langle \hat{\delta r}^2(o) \rangle [xK\sin Ks + x'\cos Ks]^2 + \langle \hat{\delta r}'^2(o) \rangle [x\cos Ks - \frac{x'}{K}\sin Ks]^2 \}, \tag{15}$$

where

$$\left.\begin{array}{l} x = \cos\left(\dfrac{\Omega_L s}{v_\theta}\right) - \cos Ks \\[3mm] x' = -\dfrac{\Omega_L}{v_\theta}\sin\left(\dfrac{\Omega_L s}{v_\theta}\right) + K\sin Ks, \end{array}\right\} \quad \text{for the r-component} \tag{16}$$

and

$$\left.\begin{array}{l} x = \sin\left(\dfrac{\Omega_L s}{v_\theta}\right) - \left(\dfrac{\Omega_L}{Kv_\theta}\right)\sin Ks \\[3mm] x' = \left(\dfrac{\Omega_L}{v_\theta}\right)\cos\dfrac{\Omega_L s}{v_\theta} - \left(\dfrac{\Omega_L}{v_\theta}\right)\cos Ks \end{array}\right\} \quad \text{for the z-component} \tag{17}$$

If the initial conditions are such that

$$K^2 \langle \hat{\delta r}^2(o) \rangle = \langle \hat{\delta r}'^2(o) \rangle,$$

Eq. (15) becomes

$$\frac{\hat{\varepsilon}^2}{16} = \langle\hat{\delta r}^2(o)\rangle\langle\hat{\delta r}'^2(o)\rangle + \delta r_o^2 K^2 \langle\hat{\delta r}^2(o)\rangle[x^2 + x'^2/K^2]. \tag{18}$$

When $\Omega_{o\theta} \gg \Omega_{oz}$, the two components of the rms emittance become

$$\frac{\hat{\varepsilon}_r^2}{16} = \langle\hat{\delta r}^2(o)\rangle\langle\hat{\delta r}'^2(o)\rangle$$

$$+ 2(\delta r_o \Omega_L/v_\theta)^2 \langle\hat{\delta r}^2(o)\rangle [1-\cos\frac{\omega^2 s}{\Omega_{o\theta}v_\theta})], \tag{19}$$

and

$$\frac{\hat{\varepsilon}_r^2}{16} = \langle\hat{\delta z}^2(o)\rangle \langle\hat{\delta z}'^2(o)\rangle$$

$$+ 2(\delta r_o \Omega_L/v_\theta)^2 \langle\hat{\delta z}^2(o)\rangle [1-\cos(\frac{\omega^2 s}{\Omega_{o\theta}v_\theta})]. \tag{20}$$

Since $\frac{\omega^2 s}{\Omega_{o\theta}v_\theta} \rightarrow o$ when $\Omega_{o\theta} \gg \omega$, the amplitude of the oscillatory terms is very small. This is contrary to the conventional betatron, in which very small energy spread results in very large oscillations of the rms emittance[12].

Results from the computer simulation with a small parallel temperature spread are shown in Fig. 7. The various parameters for this run are listed in Table IV. When a parallel energy spread is present, the matching becomes more difficult and the beam envelope starts to oscillate. These oscillations result in the growth of the ring's rms emittance and is discussed later on.

The ring dynamics in the presence of temperature is similar to that in the absence of temperature, provided that even with the expansion of the beam radius ω^2 remains different than zero. In one run the various parameters were assigned such values that ω^2 would go through zero after a small expansion of the beam radius. A very rapid increase in the beam envelope was observed that was accompanied by a 15-fold growth of the rms emittance in approximately 100 nsec. However, the expansion had no noticable effect on the macroscopic motion of the center of the beam, at least for the duration of the run.

The rms emittance as a function of time for $T_{11} \neq o$ is shown in Fig. 8a. The various parameters are listed in Table IV. The corresponding result for $T_{11} = o$ is shown in Fig. 8b. With the exception of the temperature, the various parameters for this run are identical to those listed in Table IV. Since in the numerical results

$$\langle \hat{\delta r}^2(o) \rangle = \langle \hat{\delta z}^2(o) \rangle,$$

and

$$\langle \hat{\delta r}'^2(o) \rangle = \langle \hat{\delta z}'^2(o) \rangle,$$

Equations (19) and (20) predict that when $\Omega_{o\theta} \gg \omega$

$$\epsilon_r \cong \pm \, \epsilon_z,$$

i.e., ϵ_r and ϵ_z are either in phase or approximately 180° out of phase. Fig. 8a shows that ϵ_r and ϵ_z are 180° out of phase, although the condition

$\Omega_{o\theta} \gg \omega$ is not satisfied. This appears to be a general results and has been observed in all the runs with temperature or equivalent temperature.

The secular emittance growth in Fig. 8a is attributed to the radial expansion of the ring. This is also a general result and is observed in all unmatched rings with or without temperature. Among the various non-linearities, such as field fluctuations, wall, density and radial expansion, the latter appears to be the most pronounced.

III. Conclusions

Some very preliminary experimental results[18] together with the extensive equilibrium[2-11] and stability analysis[19-24] clearly indicate that the modified betatron concept has the potential to lead to the development of very high current accelerators.

Our confidence in the modified betatron concept is further enhanced by the present results which show that the magnetic field fluctuations, that are inevitable in any practical device, appear to be harmless to the high current ring. However, the resonance that occurs when $\omega = o$ is presently a major concern.

Table I

Parameters of the run shown in Fig. 2

Run No. M14D

Initial beam energy γ_0 = 7.117

Beam current I (KA) = 5 KA

Major radius r_0 (cm) = 100

Initial beam minor radius r_b (cm) = 3

Torus minor radius a (cm) = 16

Initial beam center position r_1 (cm) = 108

Betatron magn. field at r_0, z = o, B_{oz} (G) = 136.2

Toroidal magn. field at r_0, z = o, $B_{o\theta}$ (G) = 388

Initial emittance ε (rad − cm) = 0.1

Initial temperature spread (half-width) $\frac{\Delta\gamma}{\gamma}$ = o

External field index n = 0.42 (Constant)

Self field index n_s = 1.34

Wall resistivity ρ = 0

Time step (nsec) = 100 ps

No. of particles = 1024

Table II

Parameters of the run shown in Fig. 4

Run No. M16A

Initial beam energy γ_0 = 7.117

Beam current I (KA) = 5

Major radius r_0 (cm) = 100

Initial beam minor radius r_b (cm) = 3

Torus minor radius a (cm) = 16

Initial beam center position r_i (cm) = 108

Betatron magn. field at r_0, z = o, B_{oz} (G) = 136.2

Toroidal magnetic field at r_0, z = o, $B_{o\theta}$ (G) = 388

Initial emittance ϵ (rad - cm) = 0.1

Initial temperature spread (half-width) $\frac{\Delta\gamma}{\gamma}$ = 0

External field index n = see Fig. 3

Self field index n_s = 1.34

Wall resistivity ρ = 0

Time step (nsec) = 100

No. of particles = 1024

Table III

Parameters of the run shown in Fig. 5

Run No. M05A

Initial beam energy γ_o = 6.994

Beam current I (KA) = 4.76

Major radius r_o (cm) = 100

Initial beam minor radius r_b (cm) = 3

Torus minor radius a (cm) = 16

Initial beam center position r_i (cm) = 105

Betatron magn. field at r_o, z = o B_{oz} (G) = 136.2

Toroidal magn. field at r_o, z = o, $B_{o\theta}$ (G) = 388

Initial emittance ϵ (rad - cm) = 0.1

Initial temperature spread (half-width) $\frac{\Delta\gamma}{\gamma}$ = 0

External field index n = see Fig. 3

Self field index n_s = 1.33

Wall resistivity ρ = 0

Time step (nsec) = 100 ps

No. of particles = 1024

Table IV

Parameters of the run shown in Fig. 7

Run No. J02A

Initial beam energy γ_o = 7.004

Beam current I (KA) = 5 KA

Major radius r_o (cm) = 100

Initial beam minor radius r_b (cm) = 2

Torus minor radius a (cm) = 16

Initial beam center position r_i (cm) = 105

Betatron magn. field at r_o, z = o, B_{oz} (G) = 140

Toroidal magn. field at r_o, z = o, $B_{o\theta}$ (G) = 725

Initial emittance ϵ (rad - cm) = 0.1

Initial temerpature spread (half-width) $\frac{\Delta\gamma}{\gamma}$ = 1%

External field index n = 0.42

Self field index n_s = 2.984

Wall resistivity ρ = 0

Time step (nsec) = 100 ps

No. of particles = 1024

Toroidal
Chamber

Electron
Ring

r_b

Δr

a

B_θ

ω

z

r

B^{ext}

r_0

$\Delta z + \delta z$

$\Delta r + \delta r$

$\Delta^2 = \Delta r^2 + \Delta z^2$

$r = r_0 + \Delta r + \delta r$

$z = \Delta z + \delta z$
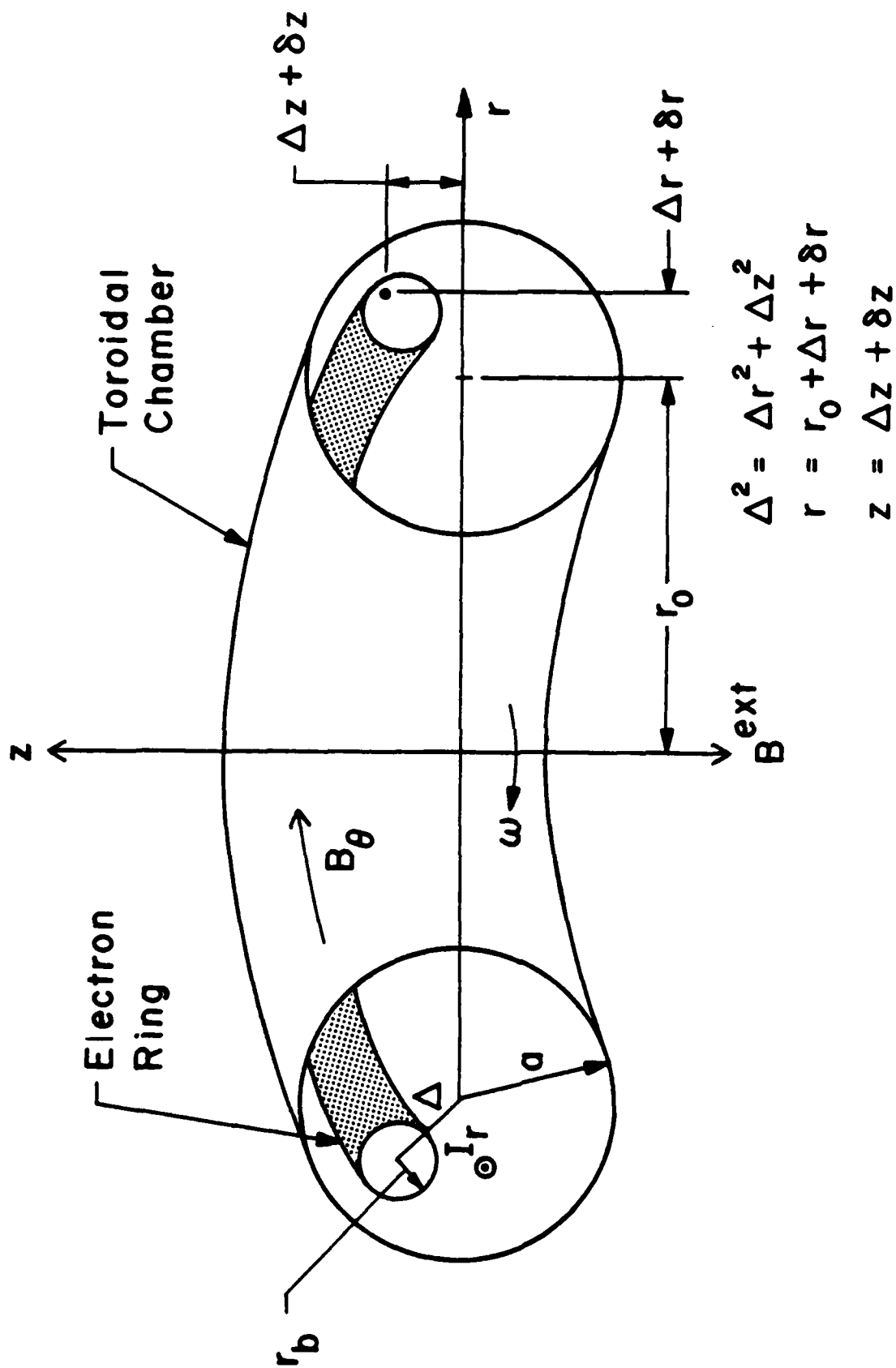
Fig. 1 Modified betatron configuration and system of coordinates.
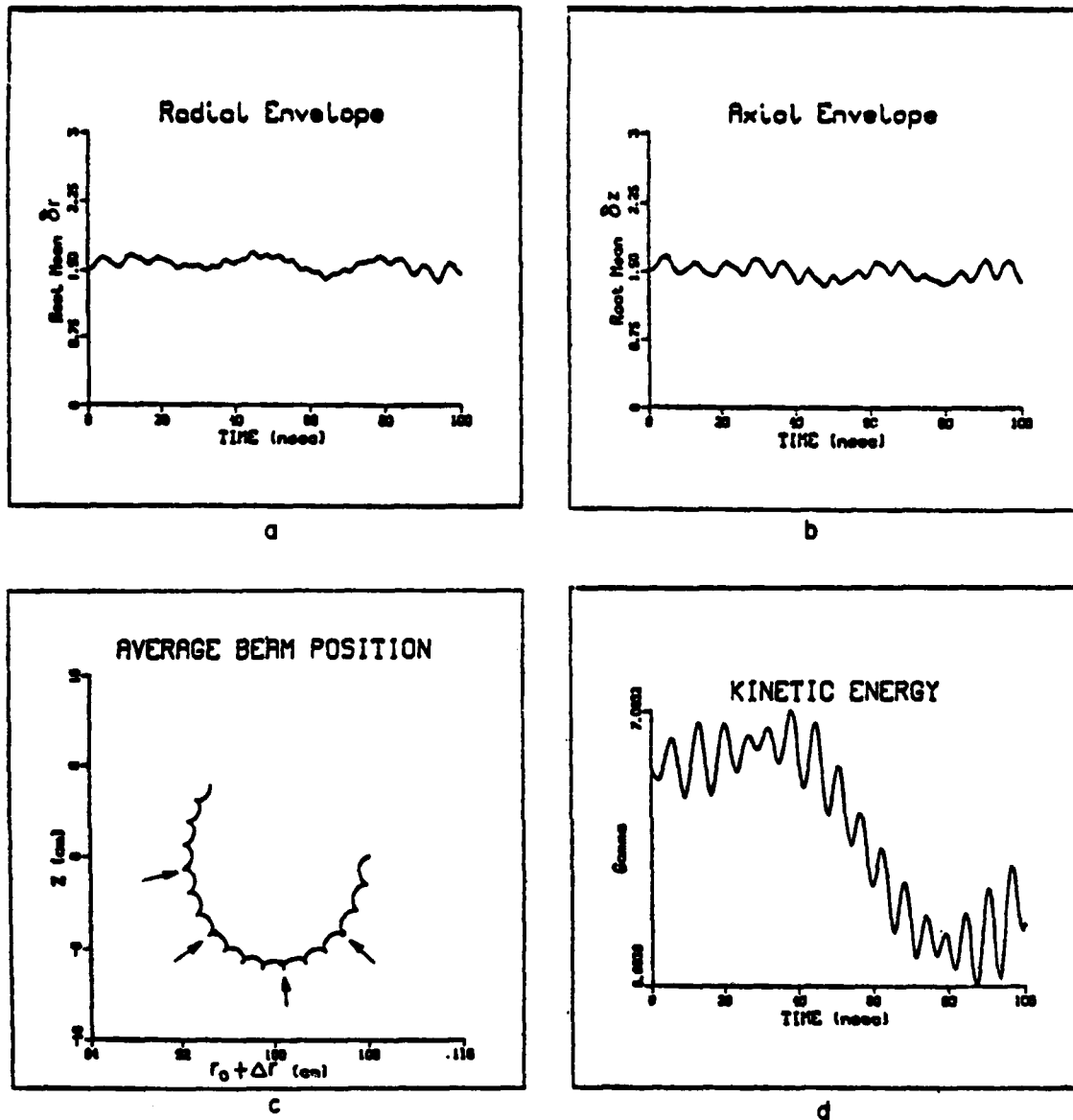
Fig. 2 (a) Temporal variation of rms radial distance of electrons from the center of the minor cross-section of the ring; (b) temporal variation of the rms vertical distance of electrons from the center of the minor cross-section of the ring; (c) orbit of the ring's center in the r-z plane; (d) temporal variation of ring's kinetic energy. In this run the external field index is uniform. The various parameters are listed in Table I.

20
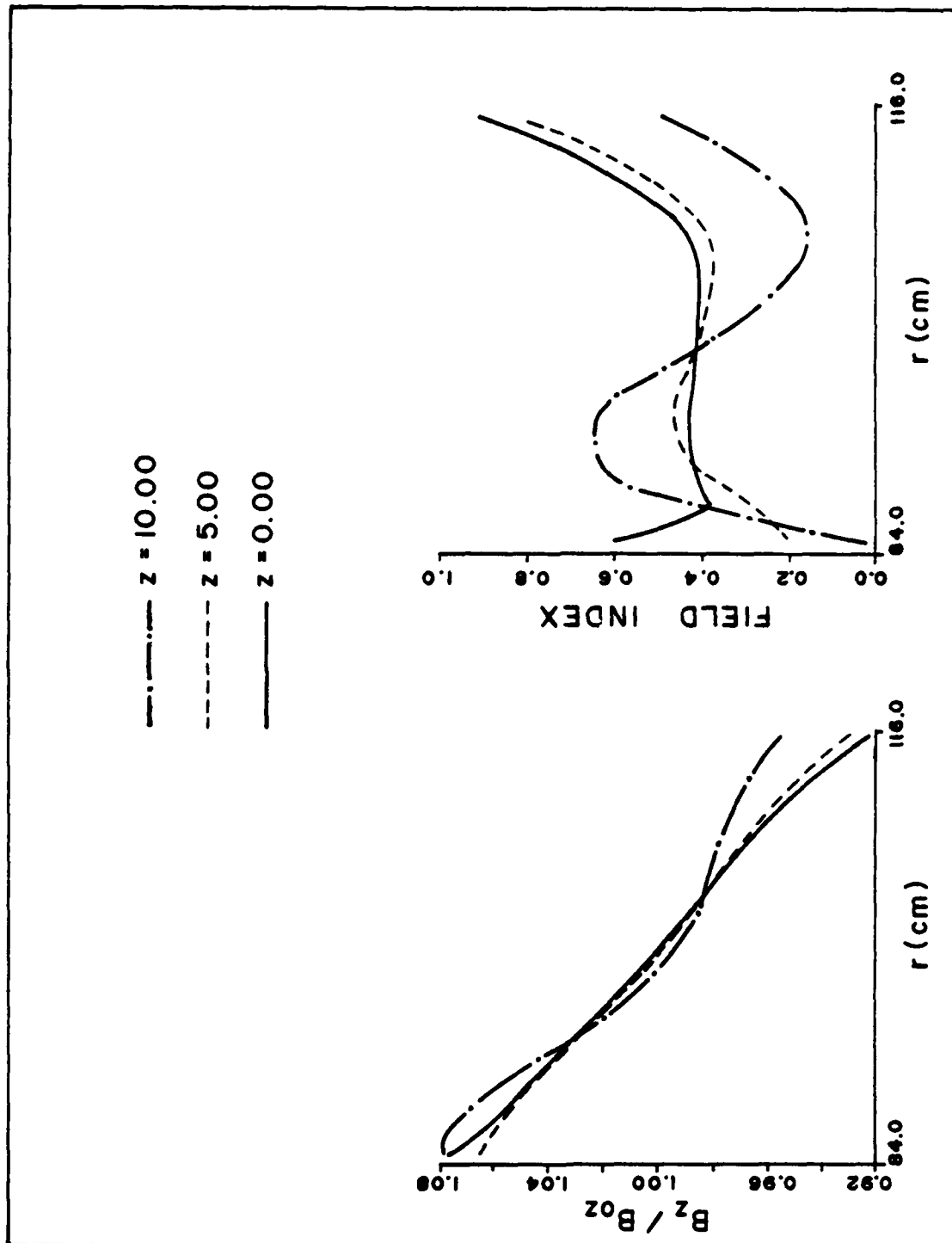
Fig. 3 Variation of the betatron magnetic field and external field index with radial distance at three vertical (z) positions.

21
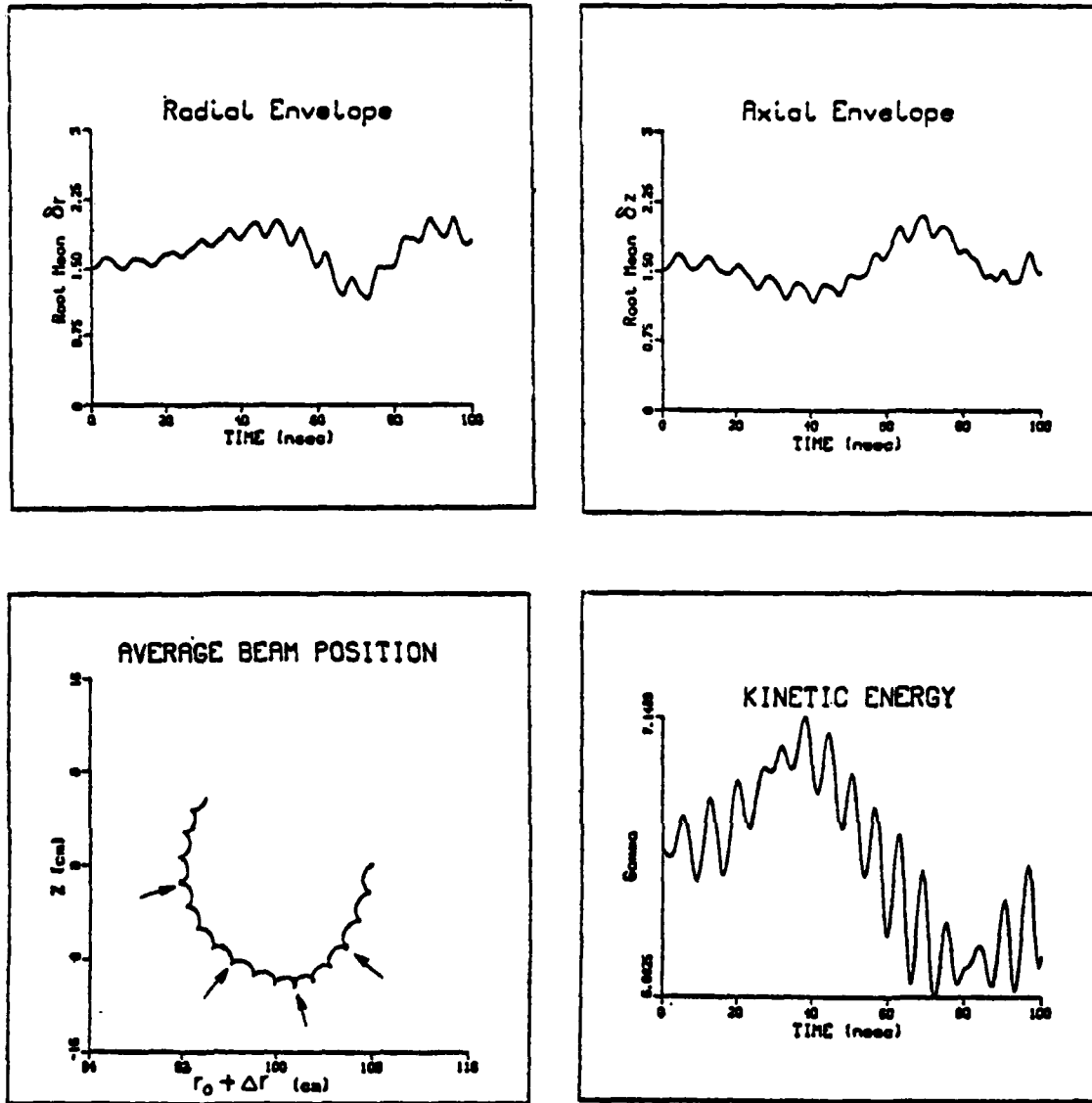
Fig. 4 (a) Temporal variation of the rms radial distance of electrons from
the center of the minor cross-section of the ring; (b) temporal
variation of the rms vertical distance of electrons from the center of
the minor cross-section of the ring; (c) orbit of the ring's center in
the r-z plane; (d) temporal variation of ring's kinetic energy. In
this run the external field index varies as shown in Fig. 3. The
various parameters are listed in Table II.

TIME - 0.00 NSEC

TIME - 25.00 NSEC

TIME - 50.00 NSEC

TIME -100.00 NSEC
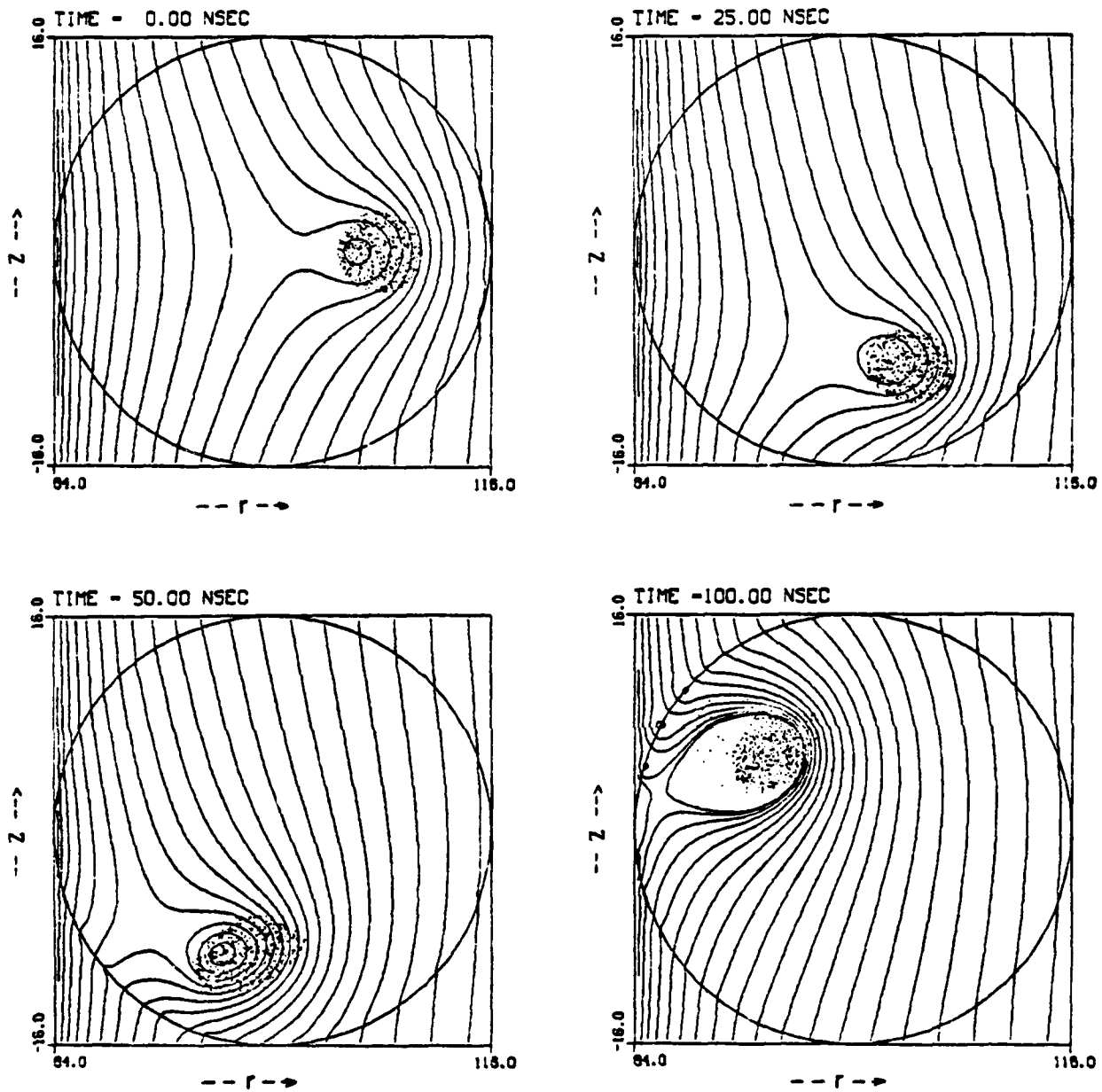
Fig. 5 Snap-shots of the electron ring minor cross-section and magnetic field

lines corresponding to the total magnetic field. The infinite

conductivity vacuum chamber has a circular minor cross-section. The

major axis of the torus is located to the left and at 100 cm from the

center of the minor cross-section of the torus. The various

parameters are listed in Table II.

23
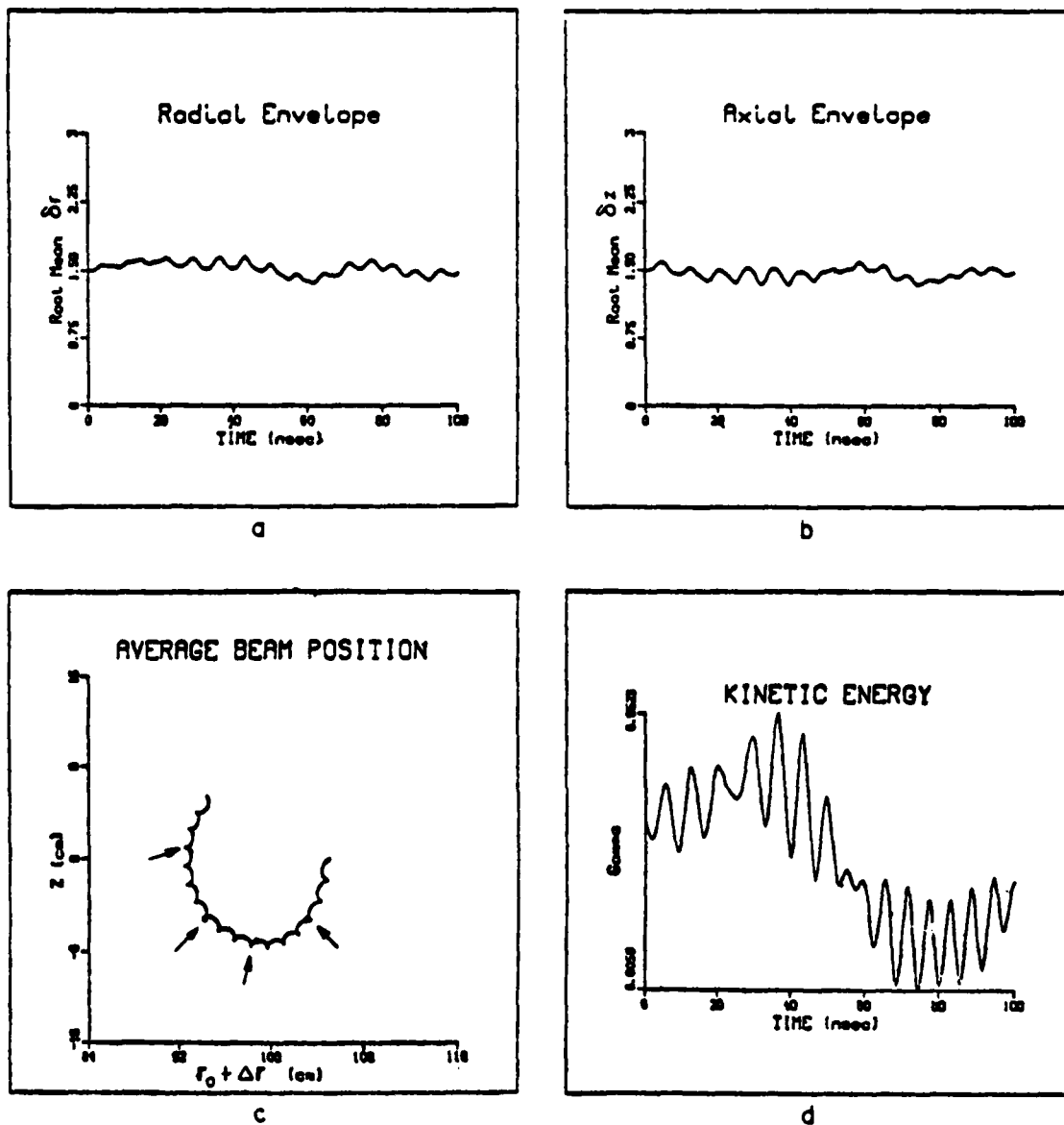
Fig. 6 (a) Temporal variation of the rms radial distance of electrons from the center of the minor cross-section of the ring; (b) temporal variation of the rms vertical distance of electrons from the center of the minor cross-section of the ring; (c) orbit of the ring's center in the r-z plane; (d) temporal variation of ring's kinetic energy. In this run the external field index varies as shown in Fig. 3. The parameters for this run are listed in Table III.

24
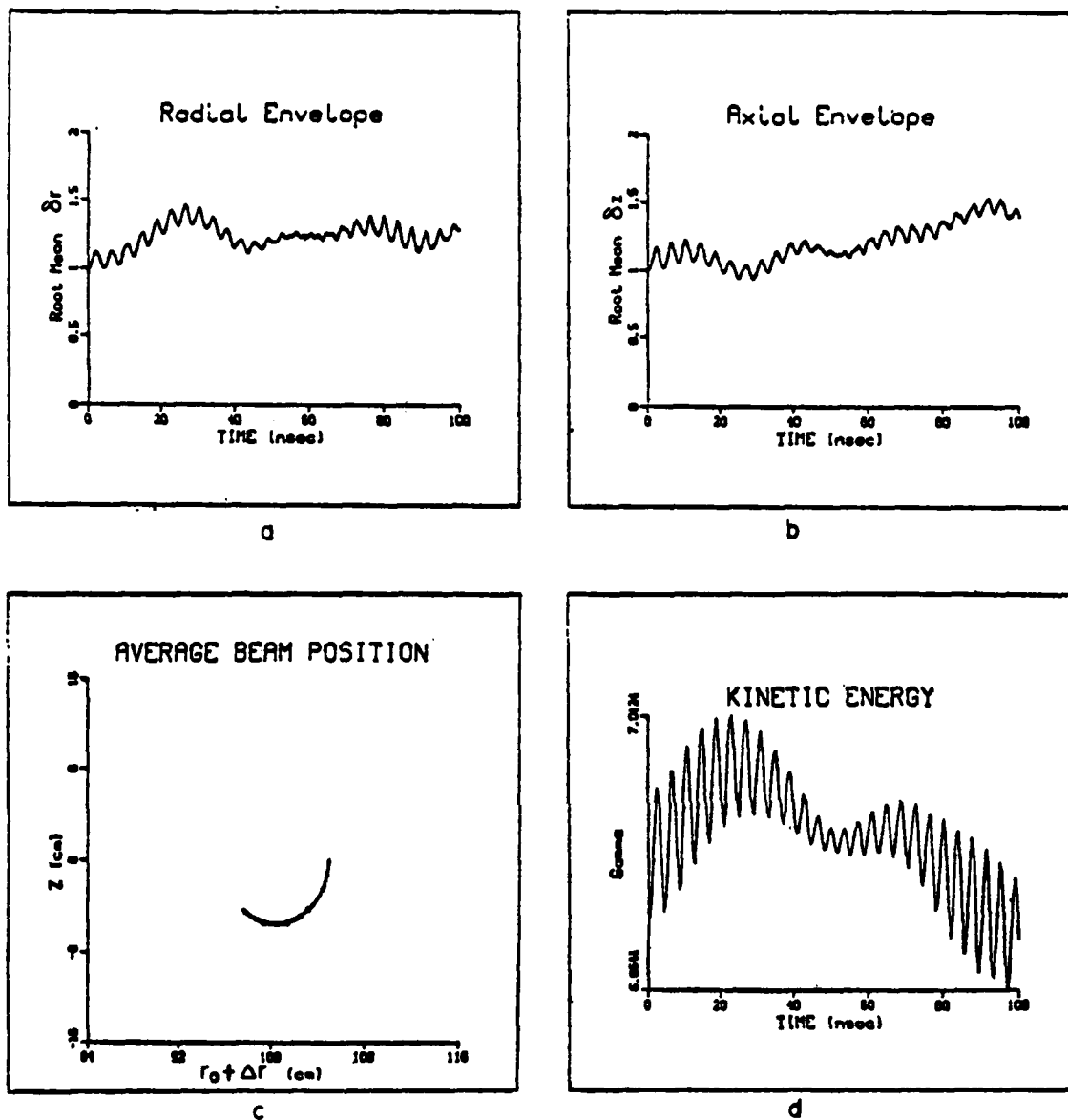
Fig. 7 (a) Temporal variation of the rms radial distance of electrons from
the center of the minor cross-section of the ring; (b) temporal
variation of the rms vertical distance of electrons from the center of
the minor cross-section of the ring; (c) orbit of the ring's center in
the r-z plane; (d) temporal variation of ring's kinetic energy. In
this run the external field index is uniform but the electrons have a
1% (half-width) temperature spread along the toroidal direction. The
various parameters for this run are listed in Table IV.

Emittance vs Time

(a)

Emittance vs Time

(b)
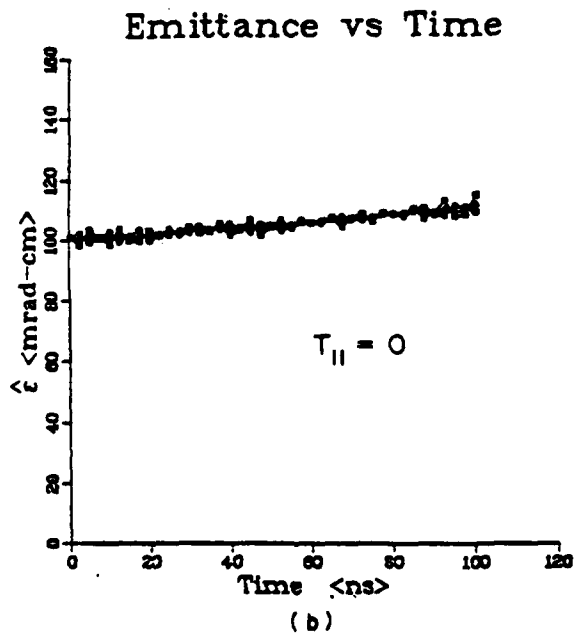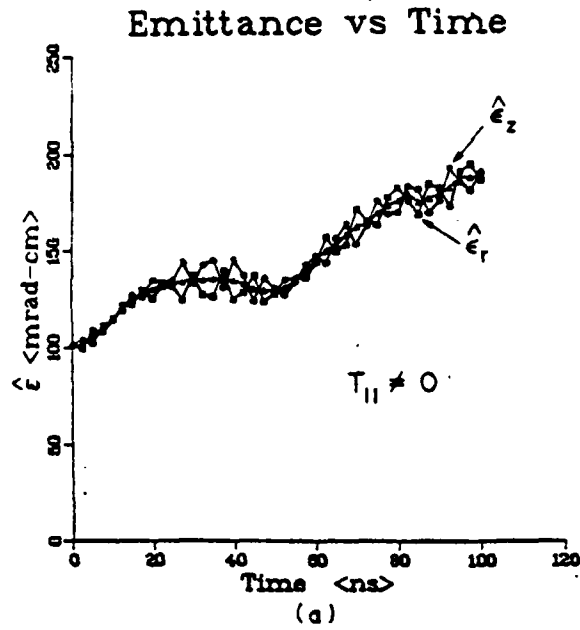
Fig. 8 (a) Temporal variation of the rms emittance ϵ_r, $\hat{\epsilon}_z$ and their average $(\hat{\epsilon}_r + \hat{\epsilon}_z)/2$, when there is a 1% (half-width) temperature spread T_{11} in the toroidal direction. The various parameters for this run are listed in Table IV; (b) as in (a) but with $T_{11} = 0$.

26

References

1. A. G. Bonch-Osmolovskii, G. V. Dolbilow, I. N. Ivanov, E. A. Perelshtein, V. P. Sarantsev, O. I. Yarkovoy, JINR-Report P9-4135 Dubna (USSR) 1968.

2. P. Sprangle and C. A. Kapetanakos, J. Appl. Phys. 49, 1 (1978).

3. N. Rostoker, Comments on Plasma Physics, Gordon and Breach Science Publ. Inc. Vol. 6, p. 91 (1980).

4. C. L. Olson and V. Schumacher Collective Ion Acceleration Springer - Verlag, Berlin, Heidelberg, New York 1979, page 199.

5. P. Sprangle, C. A. Kapetanakos and S. J. Marsh; Proc. of the Intern. Top. Conf. on High-Power Electron and Ion Beam Research and Technology; Palaiseau, France, June 29 - July 3, 1981, p. 803; Also NRL Memo Report 4666 (1981).

6. G. Barak, DD. Chernin, A. Fisher, H. Ishizuda and N. Rostoker; Proc. of the Intern. Top. Conf. on High Power Electron and Ion Beam Research and Technology; Palaiseau, France, June 29 - July 3, 1981, p. 795.

7. C. A. Kapetanakos, P. Sprangle and S. J. Marsh, NRL Memo Report 4835 (1982); also Phys. Rev. Lett. 49, 741 (1982).

8. C. A. Kapetanakos, P. Sprangle, D. P. Chernin, S. J. Marsh and I. Haber, NRL Memo Report 4905 (1982); also Phys. Fluids (June, 1983).

9. W. M. Manheimer and J. M. Finn, Particle Accelerators, 1983.

10. D. P. Chernin and P. Sprangle, Particle Accelerators 12, 85 (1982).

11. G. Barak, N. Roskoker, Phys. of Fluids 26, 3 (1983).

12. C. A. Kapetanakos, P. Sprangle and S. J. Marsh, NRL Memo Report 5108 (1983).

13. D. W. Kerst, Nature, 157, 90 (1940).

14. D. W. Kerst, et. al. Rev. Sci. Inst. 21, 462 (1950).

15. A. I. Paulovskii, et. al: Sov. Phys. Tech. Phys. 22, 218 (1977).

16. C. Roberson, A. Mondelli and D. Chernin, Phys. Rev. Lett. 50, 507 (1983).

17. D. Chernin, NRL Memo Report 5061 (1983).

18. H. H. Fleischmann, D. Taggart, M. Parker and H. J. Hopman, Particle Accel. Conf. Bull. page 146 Santa Fe, NM, 21-23 March (1983), (this ref.describes a plasma betatron, in which the elctron ring is neutralized).

19. P. Sprangle and J. Vomvoridis, NRL Memo Report 4688 (1981).

20. H. S. Uhm and R. C. Davison, MIT, Plasma Fusion Center Report No. JA-81-30 (1981).

21. R. C. Davidson and H. S. Uhm, Phys. Fluids 25, 2089 (1982).

22. T. P. Hughes and B. B. Godfrey, Mission Research Corp. Report No. AMRC-R 354, 1982; also AMRC-R-332, 1982.

23. P. Sprangle and D. Chernin, NRL Memo Report (1983).

24. P. Sprangle and C. A. Kapetanakos, NRL Memo Report 4950 (1983); also Particle Accelerators (1983).

END

FILMED

10-83

DTIC